Chapter Four *Modeling and Computational Methods*

Modeling and simulation studies in designing complex devices have become standard practice in recent years. This is crucial for preliminary device parameters study where it can reduce the cycle-time and end-product cost. There are several modeling and simulation tools that can simulate VCSELs such as PICS3D [81], HS_Design [82], SimWindows [83], ATLAS [84] and LaserMOD [85]. In this research, HS_Design Version 1.0 is used to study VCSELs DBR-mirror and active region components while LaserMOD Version 2.0 is used for complete VCSELs device characteristic simulation. This chapter provides theoretical background for the modeling and computational methods used in the simulation work of VCSELs.

4.1 Optics Calculation

The light propagation in a laser structure is determined by the solution of Maxwell's equations. The models used for optical studies are described below.

4.1.1 *Transfer Matrix Method*

Transfer Matrix Method (TMM) is employed in VCSELs optical mode calculations. The field at material interface can be separated into for- and backward-propagating plane waves. Based on Maxwell equations (frequency domain) that are [82]:

$$\begin{aligned} \nabla\times \mathrm{E}_\omega &= i\frac{\omega}{c}H_\omega, \quad \nabla\times \mathrm{H}_\omega = -i\frac{\omega}{c}\hat{k}_\omega E_\omega \\ \nabla\cdot\left(\hat{k}_\omega \mathrm{E}_\omega\right) &= 0, \qquad\qquad \nabla\cdot \mathrm{H}_\omega = 0 \end{aligned} \tag{4.1}$$

It is assumed that all the layers are homogenous in a plane perpendicular to direction of epitaxial growth (z-coordinate), the complex permittivity tensor is:

$$\hat{k}_\omega = \begin{pmatrix} \kappa_{\omega\perp} & 0 & 0 \\ 0 & \kappa_{\omega\perp} & 0 \\ 0 & 0 & \kappa_{\omega z\parallel} \end{pmatrix} \tag{4.2}$$

Here, $\kappa_{\omega\perp}$ and $\kappa_{\omega\parallel}$ are the complex permittivity in the directions perpendicular and parallel to the axis of symmetry (direction of growth), respectively. Then, in the j-th layer positioned between $z = z_{j-1} \equiv \sum_{l=0}^{j-1} d_l$ and $z = z_j \equiv \sum_{l=0}^{j} d_l$, where d_l is the width of l-th layer and widths of both the substrate ($j = 0, z < 0$) and superstrate ($j = n+1, z > z_j$) are set to zero, the vectorical fields in both the TE (electric field in the plane perpendicular to z) and TM (magnetic field in the plane perpendicular to z) polarizations can be expressed through a single scalar function:

$$\psi_{\omega,j}(r_\perp, z) = \exp(i\beta_\perp r_\perp)\left\{F_{\omega,j}\exp\left[i\beta_{zj}\left(z - z_{j-1}\right)\right] + B_{\omega,j}\exp\left[-i\beta_{z,j}\left(z - z_{j-1}\right)\right]\right\} \qquad (4.3)$$

$\beta_\perp$ is the in-plane propagation constant, $\beta_{z,j}$ is the z-direction propagation constant in j-th layer, $F_{\omega,j}$ and $B_{\omega,j}$ are the amplitudes of forward and backward propagating waves, respectively. The components of the electromagnetic field in the j-th layer are all given in the Table 4.1 for both the TE and TM polarizations. Equation (4.3) and Table 4.1 represents the exact solution of equation (4.1) in every single layer with the complex permittivity of the type equation (4.2).

Table 4.1: Propagation constant in the direction of growth and electromagnetic field.

Parameter	β_z^2	γ	$E_{\omega\perp}$	$E_{\omega z}$	$H_{\omega\perp}$	H_ω
TE-polarization	$\frac{\omega^2}{c^2}\kappa_{\omega\perp} - \beta_\perp^2$	1	ψ_ω	0	$i\frac{c}{\omega}\frac{d\psi_\omega}{dz}$	$\frac{c}{\omega}\beta_\perp\psi_\omega$
TM-polarization	$\frac{\omega^2}{c^2}\kappa_{\omega\perp} - \frac{\kappa_{\omega\perp}}{\kappa_{\omega z}}\beta_\perp^2$	$\frac{1}{\kappa_{\omega\perp}}$	$-i\frac{c}{\omega}\frac{1}{\kappa_{\omega\perp}}\frac{d\psi_\omega}{dz}$	$-\frac{c}{\omega}\beta_\perp\frac{1}{\kappa_{\omega z}}\psi_\omega$	ψ_ω	0

At the interfaces, standard boundary conditions for electric and magnetic fields yield the following transfer relationships for the scalar function (4.3) and its derivative:

$$\psi_{\omega,j} = \psi_{\omega,j-1}; \gamma_j\frac{d\psi_{\omega,j}}{dz} = \gamma_{j-1}\frac{d\psi_{\omega,j-1}}{dz} \qquad (4.4)$$

where the factor γ is defined in the Table 4.1. Combining equation (4.3) and (4.4), the amplitudes of the forward and backward waves are transfer across the interface:

$$\begin{bmatrix} F_{\omega,j} \\ B_{\omega,j} \end{bmatrix} = \hat{T}_{\omega j} \begin{bmatrix} F_{\omega,j-1} \\ B_{\omega,j-1} \end{bmatrix} \tag{4.5}$$

where $\hat{T}_{\omega j}$ is a square 2x2 complex transfer matrix:

$$\hat{T}_{\omega j} = \begin{bmatrix} \frac{1}{2}\left(1+\zeta_j\right)\exp\left(i\Delta_j\right) & \frac{1}{2}\left(1-\zeta_j\right)\exp\left(-i\Delta_j\right) \\ \frac{1}{2}\left(1-\zeta_j\right)\exp\left(i\Delta_j\right) & \frac{1}{2}\left(1+\zeta_j\right)\exp\left(-i\Delta_j\right) \end{bmatrix} \tag{4.6}$$

Information regarding the optical properties of the layers is contained in the complex parameters ζ_j and Δ_j, which are defined as follows:

$$\zeta_j = \frac{\beta_{z,j-1}\gamma_{j-1}}{\beta_{z,j}\gamma_j}, \qquad \Delta_j = \beta_{z,j} d_j \tag{4.7}$$

The amplitudes of the plane waves in superstrate and substrate are connected through multiplication of the matrixes (4.5):

$$\begin{bmatrix} F_{\omega,n+1} \\ B_{\omega,n+1} \end{bmatrix} = \hat{T}_{\omega j} \begin{bmatrix} F_{\omega,0} \\ B_{\omega,0} \end{bmatrix}, \quad \hat{T}_{\omega} = \prod_{j=1}^{n} \hat{T}_{\omega j} \tag{4.8}$$

TMM gives the optical field distribution (reflection, transmission or absorption spectrum) over the entire device once the boundary conditions of the structure are specified. The boundary conditions are formulated assuming that z-coordinate is measured up from the substrate while the light is incident down from the superstrate:

$$\begin{aligned} F_{\omega,n+1} &= r_{\omega}, & B_{\omega,n+1} &= 1 \\ F_{\omega,0} &= 0, & B_{\omega,0} &= t_{\omega} \end{aligned} \tag{4.9}$$

$F\omega$ and $B\omega$ are described as in equation (4.3), where the subscripts "$n+1$" and "0" indicating the superstrate $(z \geq z_n = \sum_{l=0}^{l=n} d_l)$ and substrate $(z \leq 0)$ with r_{ω} plus t_{ω} are the reflection and transmission amplitude coefficients, respectively. These parameters are expressed using the components of the transfer matrix defined by equation (4.5):

$$r_\omega = \frac{T_{\omega,12}}{T_{\omega,22}}, \quad t_\omega = \frac{1}{T_{\omega,22}} \tag{4.10}$$

The field distribution in every layer is given by equation (4.3), with amplitudes of the forward and backward propagating waves obtained by equations (4.5) and (4.6). The intensity coefficients of reflection and transmission are calculated as:

$$\begin{aligned} R_{\omega,VS} &= |r_\omega|^2 \\ T_{\omega,VS} &= |t_\omega|^2 \end{aligned} \tag{4.11}$$

The absorption coefficient of the vertical stack, which is defined as the fraction of light absorbed in the entire space between substrate and superstrate, is given

$$A_{\omega,VS} = 1 - T_{\omega,VS} - R_{\omega,VS} \tag{4.12}$$

4.1.1 *Phonon Rate Equation*

Optical field propagation and electro-thermal transport are coupled using rate equations for the intensity within each cavity mode [85]:

$$\frac{\partial S_{m,\omega}}{\partial t} = \left(G_{m,\omega} - \frac{1}{\tau_{m,\omega}} \right) S_{m,\omega} + R_{m,\omega}^{spon} \tag{4.13}$$

where the spontaneous emission into mode (m, ω) is given by:

$$R_{m,\omega}^{spon} = \int dV |E_m|^2 u(\omega) \tag{4.14}$$

and the modal gain is defined as:

$$G_{m,\omega} = \int dV |E_m|^2 \frac{c}{n_{eff,m}} g(\omega) \tag{4.15}$$

Here, g is the material gain; u is the spontaneous emission spectrum. The losses entering the photon rate equation are the sum of contributions due to light leaving the cavity through the facets, light scattered out the cavity and absorptive losses

$$\frac{1}{\tau_{m,\omega}} = \frac{1}{\tau_{mirror}} + \frac{1}{\tau_{scatter}} + \frac{c}{n_{eff,m}} \alpha_b \tag{4.16}$$

The absorptive losses include free-carrier absorption and inter-valence band absorption. With coefficients $k_{e/h}^{fca}$, free-carrier absorption is modeled as a linear function of the respective carrier densities:

$$\alpha_h = \int dV \left|E_m\right|^2 \left(k_e^{fca} n_e + k_h^{fca} n_h + \alpha_0\right) \tag{4.17}$$

QW barriers, cladding layers and other non-active regions in semiconductor lasers usually are designed to be transparent at the emission wavelength as given by the effective bandgap of the active layer material.

4.2 Bulk Bandstructure Calculation

As for the bulk bandstructure model, the unperturbed stationary electron states are taken as Bloch functions in the ideal crystal. The unperturbed state of electron at wave-factor $\boldsymbol{k}$ in i-th band, $|k_t, i\rangle$ is the Bloch function of the form [82]:

$$\psi_i(r) = \frac{\exp(ikr)}{\sqrt{V}} u_{ik}(r) \tag{4.18}$$

where $\boldsymbol{r}$ is the coordinate vector, V is the crystal volume, and $u_{ik}(r)$ is the periodic function of $\boldsymbol{r}$ with the same period of the crystal lattice. Doping impurities are assumed ionized and uniformly distributed over the layer. Space charge regions are ignored, and therefore, every bulk layer is assumed to be electrically quasi-neutral.

4.2.1 *Distribution Functions*

Distribution of j-th carriers over the Bloch states in the i-th band is described with a single-particle distribution function, $f_{ij}(k)$, which depends on the wave-factor $\boldsymbol{k}$. It is assumed that all the carriers in the conduction or valence band are thermalized and hence quasi-equilibrium Fermi-Dirac distribution function with common Fermi level and temperature is used to describe all electrons and holes. Then, f_{ij} is a function of energy $\varepsilon(\boldsymbol{k})$ rather than wave-factor $\boldsymbol{k}$ and written down as [82]:

$$f_{ij}(\varepsilon) = \left[1 + \exp\left(\frac{\Delta_{ij} + \varepsilon}{T_i} - \xi_i\right)\right]^{-1} \tag{4.19}$$

Here, ξ_i is the normalized chemical potential in the conduction or valence band, which is related to the Fermi levels, Φ_c and Φ_v, and band-edge energies, E_c and E_v by

$$\xi_i = \begin{cases} (\Phi_c - E_c)/T_c, & i = c \\ -(\Phi_v - E_v)/T_v, & i = v \end{cases} \tag{4.20}$$

Δij is the energy separation between the edge of i-th band and the valley minimum in the c-band or subband maximum in the v-band, from each of the energy of the j-th carriers in this band, T_i is the effective temperature of carriers in the i-th band. The ξ_i and temperature describe the free-carriers statistics under the quasi-equilibrium approximation. However, it is the carrier concentration used to characterize a semiconductor layer, typically. Thus ξ_i should be resolved from the equation below [82]

$$\sum_{(J)} \aleph_{ij,3D}(T_i) 2/\sqrt{\pi} \int_0^\infty \frac{du u^{1/2} \rho_{ij}(u)}{1+\exp(\xi_i - \Delta_{ij}/T_i - u)} = N_i \tag{4.21}$$

where $\aleph_{ij}(T_i) = 2v_{ij}\left[2\pi m_{ij} T_i/(2\pi\hbar)^2\right]^{3/2}$ is the density of states (for carriers in the conduction band, it is multiplied by the number of valleys v_{ij}), $u = \varepsilon/T_i$ and

$$\rho_{ij}(\varepsilon) = \left[\gamma_{ij}(\varepsilon)\right]^{1/2} \frac{d\gamma_{ij}(\varepsilon)}{d\varepsilon} \tag{4.22}$$

is the reduced density of states in the band with the dispersion law given by [82]:

$$\frac{\hbar^2 k^2}{2m_i} = \gamma_i(\varepsilon) = \varepsilon(1 + a_i\varepsilon) \tag{4.23}$$

where m_i and a_i are the band-edge effective mass and parameter of nonparabolicity in i-th band, and ε is the energy relative to the band edge.

When nonparabolicity is neglected, equation (4.21) is then reduces to

$$\sum_{(J)} \aleph_{ij}(T_i) F_{1/2}(\xi_i - \Delta_{ij}/T_i) = N_i \tag{4.24}$$

with $F_\alpha(y)$ as the Fermi integral (normalized to the gamma-function) defined by:

$$F_\alpha(y) = \frac{1}{\Gamma(\alpha+1)} \int_0^\infty \frac{dx x^\alpha}{1+\exp(x-y)} \tag{4.25}$$

4.2.2 *Direct Interband Transitions*

Momentum matrix element for the direct transitions between the electron states and wave-vector $\boldsymbol{k}$ in the i-th and j-th bands is determined by the sell periodic function:

$$P_{ij}(k) = \langle u_{jk} | e\hat{p} | u_{ik} \rangle \tag{4.26}$$

When squared and averaged over the solid angle 4π, for all possible interband transitions it can be expressed by a single scalar parameter, E_P, (Kane parameter) [82]:

$$\frac{1}{4\pi}\int_0^{\pi} d\vartheta \sin\vartheta \int_0^{2\pi} d\varphi \left|P_{ij}(k)\right|^2 = \frac{m_0 E_P}{6}\Pi_{ij}(k) \tag{4.27}$$

Here, $\Pi_{ij}(k)$ is the square 4x4 matrix:

$$\hat{\Pi} = \begin{bmatrix} 0 & 1 & 1 & 1 \\ 1 & 0 & 2Q^2 & (1+\chi)^{-2}Q^2 \\ 1 & 2Q^2 & 0 & (1+\chi)^{-2}Q^2 \\ 1 & (1+\chi)^{-2}Q^2 & (1+\chi)^{-2}Q^2 & 0 \end{bmatrix} \tag{4.28}$$

where $\chi = E_{so}/E_g$ that is spin-splitting energy in the valence band, E_{so} and energy gap between conduction and valence bands, E_g, respectively. The rows and columns correspond to *c*-, *vh*-, *vl*- and *vs*-bands, with Q defined as

$$Q^2 \equiv \frac{1}{3}\frac{E_P}{E_g}\frac{\hbar^2 k^2}{2m_0 E_g} \tag{4.29}$$

By replacing the sum over the states with integral over $d\varepsilon_k = d\left(\hbar^2 k^2/2\mu_{ij}\right)$, where μ_{ij} is the band-edge reduce effective mass for the pair of bands involved, the contribution from the direct interband transitions (first order process) to the imaginary part of permittivity can be written down as

$$\kappa''_{\omega,ih} = \frac{2^{3/2}e^2 E_P}{3m_0\hbar^3\omega^2}\times \tag{4.30}$$

$$\sum_{(i,j)}\mu_{ij}^{3/2}\int_0^{\infty} d\varepsilon_k \varepsilon_k^{1/2}\Pi_{ij}(\varepsilon k)\left[f_i\left[\varepsilon_i(\varepsilon_k)\right] - f_j\left[\varepsilon_j(\varepsilon_k)\right]\right]\delta_{\Gamma}\left[\Delta_{ji} + \varepsilon_j(\varepsilon_k) - \varepsilon_i(\varepsilon_k) - \hbar\omega\right]$$

where $\Delta_{ij} = -\Delta_{ji}$ is the energy gap between the i-th and j-th bands and sum of all the bands is performed. Equation (4.30) is for electrons. For holes, it is transformed to

$$\kappa''_{\omega,ib} = \frac{2^{3/2} e^2 E_p}{3 m_0 \hbar^3 \omega^2} \sum_{(j=vh,vl,vs)} \mu_{cvj}^{3/2} \times \int_0^\infty d\varepsilon_k \varepsilon_k^{1/2} \left[1 - f_{vj}\left[\varepsilon_{vj}(\varepsilon_k)\right] - f_c\left[\varepsilon_c(\varepsilon_k)\right]\right] \delta_\Gamma\left[\varepsilon_{vj}(\varepsilon_k) + \varepsilon_c(\varepsilon_k) + E_g - \hbar\omega\right] \tag{4.31}$$

for the interband transitions, with

$$\varepsilon_{vj}(\varepsilon_k) = \Delta_{vj} + \frac{\mu_{cvj}}{m_{vj}} \varepsilon_k, \quad \varepsilon_c(\varepsilon_k) = \sqrt{\frac{1}{4a_\Gamma^2} + \frac{\mu_{cvj}}{m_{c\Gamma}} \frac{\varepsilon_k}{a_\Gamma}} - \frac{1}{2a_\Gamma} \tag{4.32}$$

where nonparabolicity at Γ-valley conduction band, $a_\Gamma = \frac{(1+\chi/3)(1+\chi) + \chi^2/3}{(1+2\chi/3)(1+\chi)} \frac{1}{E_g}$,

and

$$\kappa''_{\omega,ib} = \frac{2^{3/2} e^2 E_p}{3 m_0 \hbar^3 \omega^2} \sum_{(j=vh,vl,vs)} \mu_{cvj}^{3/2} \times \int_0^\infty d\varepsilon_k \varepsilon_k^{1/2} \Pi_{ij}(\varepsilon_k) \left[f_{vi}(\varepsilon_k) - f_{vj}(\varepsilon_k)\right] \delta_\Gamma\left[\varepsilon_{vj}(\varepsilon_k) - \varepsilon_{vi}(\varepsilon_k) - \hbar\omega\right] \tag{4.33}$$

for the intervalence band transitions, with

$$\varepsilon_{vi}(\varepsilon_k) = \Delta_{vi} + \frac{\mu_{vij}}{m_{vi}} \varepsilon_k, \quad \varepsilon_{vj}(\varepsilon_k) = \Delta_{vj} + \frac{\mu_{vij}}{m_{vj}} \varepsilon_k \tag{4.34}$$

The energy gap, Δ_{vi} in equations (4.32) and (4.34) is nonzero for transitions involving the split-off valence band, for which $\Delta_{vs} = E_{so}$. Spontaneous emission is due to interband transitions from the conduction to valence bands, rather than intervalence band transitions. Then, the spectral density of this emission, which is defined as the intensity of spontaneous emission per unit volume per unit photon energy interval is:

$$I_{\omega,sp} = \frac{2^{3/2} e^2 E_p n_{ib} \omega^2}{3\pi^2 m_0 c^3 \hbar^3} \sum_{(j=vh,vl,vs)} \mu_{cvj}^{3/2} \times \int_0^\infty d\varepsilon_k \varepsilon_k^{1/2} f_{vj}\left[\varepsilon_{vj}(\varepsilon_k)\right] f_c\left[\varepsilon_c(\varepsilon_k)\right] \delta_\Gamma\left[\varepsilon_{vj}(\varepsilon_k) + \varepsilon_c(\varepsilon_k) + E_g - \hbar\omega\right] \tag{4.35}$$

4.2.3 *Incorporating Many-Body Effects*

Previous calculation does not include many-body effects (screened Coulomb interaction and exchange-correlation interaction), except for intraband scattering (through energy delta-function, δ_Γ). The Coulomb interaction between electron and hole modifies their

states as well as near band edge interband transition. To solved this, first, excitonic transition are included by adding the term

$$\kappa^{''}_{\omega,ex} = \frac{2\pi^2 e^2 E_p}{m_0 \omega^2} \times \tanh\left[\frac{1}{2}\left(\frac{\hbar\omega - E_g}{T_c} + \frac{\hbar\omega - E_g}{T_v} - \xi_c - \xi_v\right)\right] \sum_{(h,l)} \sum_{(n)} \left|\psi_{jn}\right|^2 \delta_\Gamma\left(\varepsilon_{jn} + E_g - \hbar\omega\right) \tag{4.36}$$

where ψ_{jn} and ε_{jn} are the wave-function and energy of n-th heavy-hole (j=h) or light-hole (j=l) excitonic state to the imaginary part of permittivity. Secondly, the screened Coulomb potential is replaced with the model potential of the form

$$\varphi_j(r) = -\eta_j \frac{e}{\kappa_0} \frac{\left[\exp\left(\eta_j r / a_{B,cvj}\right) - 1\right]^{-1}}{a_{B,cvj}} \tag{4.37}$$

Here, r, κ_0 and $a_{B,cvj} = \kappa_0 \hbar^2 / \mu_{cvj} e^2$ are the radial coordinate, static permittivity and effective Bohr radius, η is the fitting parameter, obtained by $\eta_j = \pi^2 a_{B,cvj} / 6 r_s$ where

$$r_s = \sqrt{\frac{\kappa_0}{4\pi e^2}} \left[\frac{1}{T_c}\frac{\partial N_c}{\partial \xi_c} + \frac{1}{T_v}\frac{\partial N_v}{\partial \xi_v}\right]^{-1/2} \tag{4.38}$$

is the radius of screening. When nonparabolicity is neglected, it is reduces to

$$r_s = \sqrt{\frac{\kappa_0}{4\pi e^2}} \left[\sum_{(J=\Gamma,X,L)} \frac{\aleph_{cj}(T_c)}{T_c} F_{-1/2}\left(\xi_c - \frac{\Delta_{cj}}{T_c}\right) + \sum_{(J=h,l,s)} \frac{\aleph_{vj}(T_v)}{T_v} F_{-1/2}\left(\xi_v - \frac{\Delta_{vj}}{T_v}\right)\right]^{\frac{1}{2}} \tag{4.39}$$

While the excitonic effects are importance at low concentrations of free carriers, the exchange-correlation interaction appears only at high carrier concentrations, resulting in bandgap shrinkage (conduction band is lowered and valence band is raised). This shifting of c- or v-band edge can be described by the local density functional method and parameterized as $V_{xc,j} = V_{xc,j}\left(N_j\right)$, or in a form as [82]

$$V_{xc,j}\left(N_j\right) = 0.0582\left\{1 + 0.7734\eta_j^{-1}\left(N_j\right)\ln\left[1 + \eta_j\left(N_j\right)\right]\right\}\eta_j\left(N_j\right)R_j, \quad {}_{j=c,vh} \tag{4.40}$$

where $\eta_j = 21\left[(4/3)\pi a_{B,j}^3 N_j\right]^{1/3}$ is the number of j-th band carriers in a spherical volume with a radius equal to their effective Bohr radius, $a_{B,j} = \kappa_0 \hbar^2 / m_j e^2$, and

$R_j = e^2/\left(2\kappa_0 a_{B,j}\right)$ is the effective Rydberg constant in that band. Then, the bandgap shrinkage is the sum of the conduction and valence band shifts [82],

$$\Delta E_{g,xc} = V_{xc,c}\left(N_c\right) + V_{xc,v}\left(N_v\right) \tag{4.41}$$

4.2.4 *Indirect Intraband Transitions*

Calculation of indirect radiative transitions before is assumpted that photon energy is above the energies of free carriers. Since the occupation numbers for the states at energy equal to or higher than $\hbar\omega \pm \hbar\Omega$ are small, it can be neglected, as well as second order process with the photon emission. Regarding to free carrier process with the absorption of photon, the imaginary part of permittivity can be reduced to

$$\kappa''_{\omega,fc} = \frac{c}{\omega}\sum_{(i)} \aleph_i\left(T_i\right)\frac{2}{\sqrt{\pi}}\int_0^{\infty} d\varepsilon \left[\frac{\gamma_i\left(\varepsilon\right)}{T_i}\right]^{1/2} \gamma_i'\left(\varepsilon\right) f_i\left(\varepsilon\right) \sum_{(j,\pm)} \sigma_{is}^{\pm}\left(\varepsilon\right) \tag{4.42}$$

where $\gamma_i\left(\varepsilon\right)$ is the function of energy define by equation (4.23), $\sigma_{is}^{\pm}\left(\varepsilon\right)$ is the cross-section of phonon absorption by the *i*-th type of carriers with absorption or emission of the *j*-th type phonon, obtaining by integrating over the phonon states written as

$$\sigma_{is}^{\pm}\left(\varepsilon\right) = \frac{2e^2}{3c\hbar^3\omega^3}\frac{1}{\sqrt{2m_i\gamma_i\left(\varepsilon\right)}}\times \tag{4.43}$$
$$\int_{q_{\min,is}^{\pm}}^{q_{\max,is}^{\pm}} \frac{dqq}{\left(1+q^{-2}r_s^{-2}\right)^2}\left\{\frac{\hbar^2 q^2}{2m_i\gamma_i'\left(\varepsilon\right)} - \left[\frac{m_j\gamma_j'\left(\varepsilon_s^{\pm}\right)}{m_i\gamma_i'\left(\varepsilon\right)} - 1\right]\left[\frac{\gamma_j\left(\varepsilon_s^{\pm}\right)}{\gamma_j'\left(\varepsilon_s^{\pm}\right)} - \frac{\gamma_i\left(\varepsilon\right)}{\gamma_i'\left(\varepsilon\right)}\right]\right\} G_{is}^{\pm}\left(q,\varepsilon\right) W_{is}^{\pm}\left(q\right)$$

Here, $\varepsilon_s^{\pm} = \varepsilon - \Delta_{ji} + \hbar\omega \pm \hbar\Omega_{sq}$ is the carrier energy after transition with phonon "s" at wave-vector q and energy $\hbar\Omega_{sq}$, resulting in change of carrier type and energy separation in the band structure $\Delta_{ji} = -\Delta_{ij}$ for $\varepsilon_s^{\pm}$. Then, $q_{\min,is}^{\pm}$ and $q_{\max,is}^{\pm}$ as limits of integral in equation (4.31) are the lower and upper values wave-number given by

$$q_{\min,is}^{\pm} = \frac{1}{\hbar}\left[\sqrt{2m_j\gamma_j\left(\varepsilon_s^{\pm}\right)} - \sqrt{2m_i\gamma_i\left(\varepsilon\right)}\right], q_{\max,is}^{\pm} = \frac{1}{\hbar}\left[\sqrt{2m_j\gamma_j\left(\varepsilon_s^{\pm}\right)} + \sqrt{2m_i\gamma_i\left(\varepsilon\right)}\right] \tag{4.44}$$

$G_{is}^{\pm}(q,\varepsilon)$ and $W_{is}^{\pm}(q)$ in equation (4.32) are the squared overlap integrals of the Bloch functions and matrix element for the unscreened electron-phonon interaction. If nonparabolicity is neglected, the $\sigma_{is}^{\pm}(\varepsilon)$ is reduces to

$$\sigma_{is}^{\pm}(\varepsilon)=\frac{2e^2}{3c\hbar^3\omega^3}\frac{1}{\sqrt{2m_i\varepsilon}}\times \int_{q_{min,s}^{\pm}}^{q_{max,s}^{\pm}}\frac{dqq}{\left(1+q^{-2}r_s^{-2}\right)^2}\left[\frac{\hbar^2q^2}{2m_i}-\left(\frac{m_j}{m_i}-1\right)\left(\hbar\omega-\Delta_{js}\pm\hbar\Omega_{sq}\right)\right]W_{is}^{\pm}(q) \tag{4.45}$$

In the high-frequency limit, the photon energy is far above the energies of electrons or holes (thus not dependent on energy), resulting a simple relationship for a free carrier contribution to the imaginary part of permittivity:

$$\kappa_{w,fc}^{''}\cong\frac{\omega}{c}\sum_{(i)}N_i\sum_{(s)}\Xi_{is} \tag{4.46}$$

where Ξ_{is} the characteristic cross-section of absorption given in [86] by the *i*-th carrier with scattering by the *s*-th type phonon. This can be applied for impurity scattering with the energy $\hbar\Omega_{sq}$ set to zero, as well as other types of scattering [86].

4.3 Quantum Well (QW) Calculation

In order to model QW, the bandstructure is calculated using KP perturbation theory. QW is made by growing a thin layer of narrower bandgap semiconductor within a wider bandgap semiconductor, where the inserted layers are thin enough to cause quantum confinement of the carriers. The bandgap structure is shown in Figure 4.1(a). The narrower bandgap layer is treated as potential wall for both the electrons and holes. Active region may contain multi-QW as shown in Figure 4.1(b).

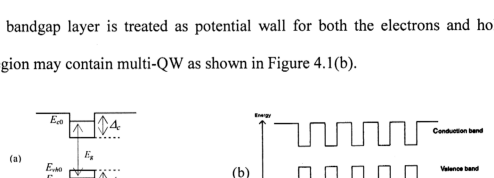

Figure 4.1: Schematic energy band diagram of a (a) QW and (b) MQW.

The quantum subband structure is based on isolated square QW with parabolic band approximation of Kane model. The single conduction band and three valence bands in the Brillouin zone center are described by the wave function of the form [82]

$$\psi_i(z,r) = \psi_{ik}(z)\frac{\exp(ikr)}{\sqrt{A}}u_i(z,r) \tag{4.47}$$

where z, r and k are the coordinate in the direction of growth, in-plane vector coordinate and in-plane wave-vector. ψ_{ik} is the envelope function, u_i is the periodic cell function and A is the area of QW. The ψ_{ik} function for the i-th band carrier is found by solving the Schrödinger equation with the Ben Daniel-Duke Hamiltonian [82]:

$$-\frac{\hbar^2}{2}\left[\frac{d}{dz}\frac{1}{m_{iz}(z)}\frac{d}{dz}\right]\psi_{ik}(z)+\left[V_i(z)-\frac{\hbar^2k^2}{2m_{i\perp}(z)}-\varepsilon_i\right]\psi_{ik}(z)=0 \tag{4.48}$$

with $m_{iz}(z)$ and $m_{i\perp}(z)$ are the effective masses in the directions parallel and perpendicular to the growth direction (associated with z-coordinate), $V_i(z)$ and ε_i are the potential and total energies of the i-th band carrier (from band edge in the well). For a square QW, the potential energy profile is taken as

$$V_i(z) = \Delta_i \vartheta(|z|-d_w) \tag{4.49}$$

where $\Delta_i > 0$ is the barrier of i-th band carrier, d_w is the half-width of QW and $\vartheta(x)$ is the unitary step-function. Equation (4.48) is reduces to the continuity of ψ_i and $(1/m_i)\times d\psi_i/dz$ with boundary conditions of heterojunction interfaces at $z=\pm d_w$. Away from QW, the boundary conditions depend on the bound (2D) or unbound (3D) state. By introducing the kinetic energy of the motion in the plane of QW [82],

$$\varepsilon_{ik} = \frac{\hbar^2k^2}{2m_{i\perp\omega}} \tag{4.50}$$

where $m_{i\perp\omega}$ stands for in-plane effective mass in the well layer. 2D and 3D states are separated by inequalities [82]:

$$\begin{aligned} &\varepsilon_{ik} < \varepsilon_i < \Delta_i + \zeta_{i\perp}\varepsilon_{ik} \quad ,2D \quad states \\ &\varepsilon_i > \Delta_i + \zeta_{i\perp}\varepsilon_{ik} > \varepsilon_{ik} \quad ,3D \quad states \end{aligned} \tag{4.51}$$

Here, $\zeta_{i\perp} = m_{i\perp w}/m_{i\perp b} < 1$ is well-to-barrier in-plane effective mass ratio (subscripts "*w*" and "*b*" indicate the well and barrier). This ratio is less than unity since the well layer has narrower bandgap compared to the barrier layer. The *i*-th band carrier at wave-number *k* sees this effective mass mismatch as a reduction of the potential barrier by the value $(1-\zeta_{i\perp})\varepsilon_{ik}$. The 2D states are possible within the interval

$$0 \le k \le \frac{1}{\hbar}\sqrt{\frac{2m_{i\perp w}\Delta_i}{1-\zeta_{i\perp}}} \tag{4.52}$$

and obtained as the solutions of eq.(4.48) with boundary conditions away from QW: $\psi_i(\pm\infty) = 0$. Due to a spatial symmetry of the potential, $V_i(-z) = V_i(z)$ the allowed states are either even: $\psi_i(-z) = \psi_i(z)$ or odd: $\psi_i(-z) = -\psi_i(z)$ states. The total energy of the band edge in well layer, ε_i is given from the dispersion equations [82]:

$$\begin{aligned} \zeta_{iz}(q_{ib}/q_{iw}) &= \tan(q_{iw}) \quad : even \quad state \\ \zeta_{iz}(q_{ib}/q_{iw}) &= -\cot(q_{iw}) \quad : odd \quad state \end{aligned} \tag{4.53}$$

where q_{iw} and q_{ib} are the parameters defined as

$$\begin{aligned} q_{iw} &= d_w/\hbar\sqrt{2m_{izw}(\varepsilon_i - \varepsilon_{ik})} \\ q_{ib} &= d_w/\hbar\sqrt{2m_{izb}(\Delta_i - \varepsilon_i + \zeta_{i\perp} - \varepsilon_{ik})} \end{aligned} \tag{4.54}$$

Altogether, there are $\mathfrak{I}_{i,ev}$ even and $\mathfrak{I}_{i,od}$ odd subbands,

$$\begin{aligned} \mathfrak{I}_{i,ev} &= 1 + \mathrm{int}\left(\frac{d_w}{\pi\hbar}\sqrt{2m_{izw}\left[\Delta_i - (1-\zeta_{i\perp})\varepsilon_{ik}\right]}\right) \\ \mathfrak{I}_{i,od} &= \mathrm{int}\left(\frac{1}{2} + \frac{d_w}{\pi\hbar}\sqrt{2m_{izw}\left[\Delta_i - (1-\zeta_{i\perp})\varepsilon_{ik}\right]}\right) \end{aligned} \tag{4.55}$$

The spectrum $\varepsilon_{ij(k)}$ of each subband is different from a parabolic case, $\varepsilon_{ij}(k) = E_{ij} + \varepsilon_{ik}$ when the effective mass mismatch is considered. Subscripts "*j*" indicates the number of subband in *i*-th band and $E_{ij} = \in_{ij}(0) > 0$ is the quantum subband edge. There is always at least one even subband and the wider and deeper the QW, the more number of quantum subbands it supports. However, no 2D states at all

are possible if $\varepsilon_{ik} > \Delta_i/(1-\zeta_{i\perp})$. Envelope functions of the 2D states in the isolated square QW can be calculated using normalization

$$\int_{-\infty}^{\infty} \psi_{ij'k}^{*}(z)\psi_{ijk}(z)dz = \delta_{jj'} \tag{4.56}$$

The quantum confinement factor $\Gamma_{ij}(k)$ is given by

$$\Gamma_{ij}(k) \equiv \int_{-d_w}^{d_w} |\psi_{ijk}(z)|^2 = \tag{4.57}$$

$$\left\{1+\zeta_{iz}\frac{q_{ijb}(k)}{q_{ijw}(k)}\left[1+\zeta_{iz}\frac{q_{ijb}^2(k)}{q_{ijw}^2(k)}\right]^{-1}\right\}\left\{1+\frac{1}{q_{ijb}(k)}\left[1+\zeta_{iz}\frac{q_{ijb}^2(k)}{q_{ijw}^2(k)}\right]\left[1+\zeta_{iz}^2\frac{q_{ijb}^2(k)}{q_{ijw}^2(k)}\right]^{-1}\right\}^{-1}$$

Here, $q_{ijw}(k)$ and $q_{ijb}(k)$ are the normalized wave-numbers in the well and barriers obtained by replacing ε_i with $\varepsilon_{ij}(k)$ in the upper and lower of equation (4.54). Then, the reduced density of states in the 2D subband, $\rho_{ij}(k)$ is given by

$$\rho_{ij}(k) \equiv \frac{d\varepsilon_{ik}}{d\varepsilon_i(k)} = \left\{1-(1-\zeta_{i\perp})\left[1+\zeta_{iz}\frac{q_{ijb}^2(k)}{q_{ijw}^2(k)}+q_{ijb}(k)\left(1+\zeta_{iz}^2\frac{q_{ijb}^2(k)}{q_{ijw}^2(k)}\right)\right]^{-1}\right\}^{-1} \tag{4.58}$$

Bandgap shrinkage in a QW is due to the exchange-correlation interaction of free carriers, similar in the bulk semiconductor. The approach is similar to equation (4.29). It is assumed that this interaction shifts down the conduction band edge and shifts up the valence band edges, seen as an increase in the barrier height given by

$$\Delta_{i,xc}(N_{i,eff}) = 0.0582\left\{1+0.7734\eta_i^{-1}(N_{i,eff})\ln\left[1+\eta_i(N_{i,eff})\right]\right\}\eta_i(N_{i,eff})R_i \tag{4.59}$$

Here, $N_{i,eff}$ is the effective bulk concentration of the *i*-th band carriers in the well. With the corrections due to the strain and exchange-correlation interaction, the barrier height seen by the *i*-th band carrier is

$$\Delta_i = \Delta E_i + \Delta_{i,str} + \Delta_{i,xc} \tag{4.60}$$

where ΔE_i is the band offset at heterojunction in a QW.

4.4 Strain Effect Calculation

In semiconductor lasers, strained layer forms the QWs in the active region. Strain is due to the lattice mismatch between the epitaxial layers and substrate. Figure 4.2 shows a schematic interface of two materials (A and B) where the atoms are not match properly and some left with incomplete bonds. The larger atoms in material A are spaced apart, thus, atoms at the interface have three rather than the standard four crystal bonds. These incomplete bonded atoms can degrade the electrical properties of the device near the interface.

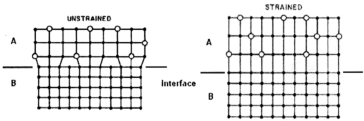

Figure 4.2: A schematic unstrained and strained-layer.

Semiconductor layers can accommodate the strain of lattice mismatch of more than one percent without forming the misfit dislocations which degrade the performance. It gives flexibility in selecting materials, enabling designing of devices not possible if following strict lattice-matching requirements. New wavelength laser emission can also be generated. Strain leads to renormalization of the energy bands. As a function of the lattice constants of the strained crystal with respect to the reference unstrained material, a_{ref} energy shifts due to shear forces is given by [85]

$$\delta E_{shear} = b\left(1+2\frac{c_{12}}{c_{11}}\right)\frac{a-a_{ref}}{a_{ref}} \tag{4.61}$$

and hydrostatic strain given by

$$\delta E_{hydro} = 2a_{cv}\left(1-\frac{c_{12}}{c_{11}}\right)\frac{a-a_{ref}}{a_{ref}} \tag{4.62}$$

occur as diagonal renormalizations in equation (4.18), where b is axial deformation potential, a_{cv} is hydrostatic deformation potential, c_{11} and c_{12} are elastic stiffness

constants. Within the parabolic band approximation, strain is assumed as band edge shift. Considered the relative change in the lattice constant, $\delta = (a - a_0)/a_0$, where a_0 and a are the lattice constants of the substrate and well. Assuming that the barriers are lattice-matched to the substrate, the shift in the band edge in the well is seen as an addition $\Delta_{i,str}$ to the barrier height, which is proportional to δ. The expressions for these parameters in the conduction, heavy hole and light hole bands follow from directly from the Pikus-Bir Hamiltonian and can be written down as

$$\begin{aligned}
\Delta_{c,str} &= 2A_c\left(1 - C_{12}/C_{11}\right)\times\delta \\
\Delta_{vh,str} &= -\left[2A_v + B - 2\left(A_v - B\right)C_{12}/C_{11}\right]\times\delta \\
\Delta_{vl,str} &= -\left[2A_v - B - 2\left(A_v + B\right)C_{12}/C_{11}\right]\times\delta
\end{aligned} \tag{4.63}$$

where A_c, A_v and B are the deformation potentials for the conduction and valence bands, C_{11} and C_{12} are the elastic constants.

4.5 Carrier Transport Calculation

The drift-diffusion system of equations which consists of carrier continuity equations and Poisson equation are applied for carrier transport calculation. Lattice heat equation is used to describe self-heating effects. As for transport across hetero-interfaces, it is based on thermionic emission. A 2D device cross-section is rendered with rectangular elements. A material system, alloy composition and doping are then selected. The cross-section is digitized with a non-uniform (Delauney) mesh. The transport equations are then solved using Gummel & Newton-Raphson Iteration [85].

4.5.1 *Poisson Equation and Charges*

The electric potential Φ is determined by Poisson equation, where the charges are given by the densities of electrons n_e and holes n_h, q is the elementary charge, and ε is the static dielectric permittivity based on the material parameter [85]

$$\nabla \varepsilon \nabla \phi = q\left(n_e + n_h - N_D^+ + N_A^-\right) \tag{4.64}$$

The ionized donors N_D^+ and acceptors N_A^- are defined by

$$N_D^+ = \frac{N_D}{1 + g_D \exp\left(\frac{F_e - E_D}{k_B T}\right)} \quad , \quad N_A^- = \frac{N_A}{1 + g_A \exp\left(\frac{E_A - F_h}{k_B T}\right)} \tag{4.65}$$

The dopant degeneracy factors are typically g_D=2 and g_A=4. The activation energies for donors E_D and acceptors E_A are based on the material parameter. $F_{e/h}$ is the Fermi energies for electrons and holes respectively.

4.5.2 *Carrier Distribution and Wavefunctions*

In QWs, the confinement potential leads to localized bound states, while propagating states exist for energy higher than the barrier band edge. The propagating states are based on classical approach for bulk regions. Quantum mechanical model is applied for bound states. By using envelope function approximation [85], the spatial distribution of carriers in the QW confined direction is described by wavefunctions ψ_j

$$n_{2D}(y) = \sum_j \left|\psi_j(y)\right|^2 \int_{E_m}^{\infty} g_{2D,j}(E) f(E) dE \tag{4.66}$$

which are obtained by solving a 1D Schrödinger equation and assuming the growth direction is in the y-axis:

$$-\left(\frac{\hbar^2}{2m_{e/h}}\frac{d^2}{dy^2} - V_{e/h}(y)\right)\psi_j(y) = E_j \psi_j(y) \tag{4.67}$$

The bound carrier densities are determined by integrating over the occupation probability as given by the Fermi distribution function $f(E)$ and the density of states g_{2Dj} for sub-band j, which results from the bandstructure calculation. $m_{e/h}$ are the electrons and holes masses respectively. While the bulk masses are depending on the material parameter, the masses for bound QW electrons and holes are determined from the bandstructure KP calculation. The confinement potential for electrons and holes, $V_{e/h}$ consist offsets of conduction and valence bands as well as the electric potential. Carrier

density dependent bandgap renormalizations that are derived from local density approximation for the Coulomb self-energies are also included in the band edges. By solving equation (4.67), sub-band energies E_j for sub-band j, and the respective wavefunctions are obtained. Finally, the total carrier concentrations is given by the sum of carriers in bound states and propagating continuum states, $n_{e/h}=n_{e/h}^{2D}+n_{e/h}^{3D}$. The bound carriers are the sum over individual sub-band contributions. In bulk regions, the carrier densities are related to the Fermi levels by

$$n_{e/h}^{3D}=2\left(\frac{m_{e/h}k_BT}{2\pi\hbar^2}\right)^{3/2}F_{1/2}\left(\frac{\pm F_{e/h}\mp E_{C/V}}{k_BT}\right)=N_{C/V}^{eff}F_{1/2}\left(\frac{\pm F_{e/h}\mp E_{C/V}}{k_BT}\right) \qquad (4.68)$$

where $F_{1/2}$ is the Fermi integral of order one-half, $F_{e/h}$ are the Fermi energies of electrons and holes, and $E_{C/V}$ are the conduction and valence band edges.

4.5.3 *Carrier Continuity Equations*

In QW, separate continuity equations are solved for bound and continuum states to describe incomplete capture of carriers. Figure 4.3 illustrates the transport model inside the QW where A is bulk drift-diffusion current, B is transport into QW continuum states, C is carrier capture and escape, D is non-radiative recombination from continuum states and E is radiative (stimulated/spontaneous) and non-radiative recombination from bound QW states [87].

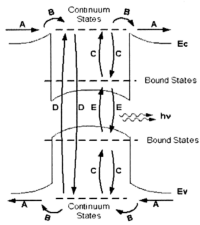

Figure 4.3: Schematic illustration of the transport model [85].

Capture due to carrier-carrier and carrier-phonon scattering will couple the classical propagating bulk and QW continuum states to quantum confined bound states. For fast inter sub-band scattering leading to thermalization between the sub-bands, the occupation of the individual sub-band can be described by a common Fermi level. This reduces the set of rate equations to a four level system defined by effective rates and density of states, which are the sum of the sub-band contributions [85].

$$q\frac{\partial n_{e/h}^{2D}}{\partial t} = \pm\nabla J_{e/h,\|} - qR^{dark} - qR^{stim} - qR^{spon,bound} + qR_{e/h}^{capture} \tag{4.69}$$

$$q\frac{\partial n_{e/h}^{3D}}{\partial t} = \pm\nabla J_{e/h} - qR^{dark} - qR^{spon,bulk} - qR_{e/h}^{capture} \tag{4.70}$$

where $R_{e/h}^{capture}$ is the capture rates for electrons and holes, R^{dark} is non-radiative recombination rate, $R^{spon,bound}$ and $R^{spon,bulk}$ are the spontaneous recombination rates for bound and bulk carriers, R^{stim} is the stimulated recombination rate. $J_{e/h}$ and $J_{e/h,\|}$ describe the currents. For bound states, only carrier flux within the QW plane indicated by $\|$ is considered, since the carrier distribution in the growth direction is determined by the wavefunctions within the confinement potential.

4.5.4 *Quantum Well Carrier Capture*

Capture into and escape from bound states is described by Maser equation rates [85] for in- and out-scattering. The capture rate $R_{e/h}^{capture} = R_{e/h}^{capture,cc} + R_{e/h}^{capture,ph}$ is the sum of contributions due to carrier-carrier and carrier-phonon scattering.

$$R_{e/h}^{capture,cc} = \int dE \int dE' g_{e/h}^{3D}(E) g_{e/h}^{2D}(E') \times \tag{4.71}$$
$$\left(s_{e/h}^{capture,cc}(E,E') f_{e/h}^{3D}(E)\left(1-f_{e/h}^{2D}(E')\right) - s_{e/h}^{escape,cc}(E,E')\left(1-f_{e/h}^{3D}(E)\right) f_{e/h}^{2D}(E')\right)$$

$$R_{e/h}^{capture,ph} = \int dE \int dE' g_{e/h}^{3D}(E) g_{e/h}^{2D}(E') \times \tag{4.72}$$
$$\left(s_{e/h}^{capture,ph}(E,E')\left(n_{ph}+1\right) f_{e/h}^{3D}(E)\left(1-f_{e/h}^{2D}(E')\right) - s_{e/h}^{escape,ph}(E,E') n_{ph}\left(1-f_{e/h}^{3D}(E)\right) f_{e/h}^{2D}(E')\right)$$

The scattering coefficients $s_{e/h}^{capture/escape,cc/ph}$ are assumed to depend on the occupation of the involved states resulting from a quantum kinetic treatment of the scattering process

in term of quantum Boltzmann equations. These scattering coefficients are given by constant rates normalized by the final density of states [87]. Due to emission and absorption of longitudinal optical (LO) phonons, capture due to phonon scattering allows continuum states to interact with non-resonant bound states which is contrast to Coulomb scattering process where the energy is conserved. The phonon occupation number is given below where ω_{LO} is the LO phonon frequency [85].

$$n_{ph} = \left(\exp\left(\frac{\hbar\omega_{LO}}{k_B T_{latt}} \right) - 1 \right)^{-1} \tag{4.73}$$

4.5.5 *Auger Recombination*

The non-radiative recombination R^{dark} occurs in both bulk and QWs regions. The rate is the sum of contributions due to Auger and Shockley-Read-Hall (SRH) processes. In the Auger process, an electron and hole recombine with the energy is transferred to an additional electron or hole. The Auger recombination is modeled by [85]

$$R^{Auger} = \left(C_e^{Auger} n_e + C_h^{Auger} n_h \right) \left(n_e n_h - n_i^2 \right) \tag{4.74}$$

where n_i is the intrinsic carrier density. The Auger coefficients are temperature dependent, described below. The temperature dependent is characterized by activation energy $E_{e/h}^{Auger,act}$ based on the material parameter.

$$C_{e/h}^{Auger}(T) = C_{e/h}^{Auger}(300K) \exp\left(-E_{e/h}^{Auger,act} \left(\frac{1}{k_B T} - \frac{1}{k_B 300K} \right) \right) \tag{4.75}$$

4.5.6 *Shockley-Read-Hall (SRH) Recombination*

SRH process describes recombination through trap levels. The rate is modeled by [85]

$$R^{SRH} = \frac{n_e n_h - n_i^2}{\tau_h^{SRH}\left(n_e + n_e^{trap} \right) + \tau_e^{SRH}\left(n_h + n_h^{trap} \right)} \tag{4.76}$$

The lifetimes τ_n^{SRH} and τ_p^{SRH} for electrons and holes, and trap energy E_{trap} are based on the material parameter with the trap occupations $n_{e/h}^{trap}$ are given by

$$n_{e/h}^{trap} = N_{C/V}^{eff} F_{1/2}\left(\frac{\pm E_{trap} \mp E_{C/V}}{k_B T}\right) \tag{4.77}$$

4.5.7 *Interface Trap Recombination*

Deep level trap can be associated with material interfaces. In the interface recombination model, the interface recombination rate (per surface area) is given by

$$R^{iface-SRH} = \frac{n_e n_h - n_i^2}{\frac{1}{v_h^{iface-SRH}\left(n_e + n_e^{trap}\right)} + \frac{1}{v_e^{iface-SRH}\left(n_h + n_h^{trap}\right)}} \tag{4.78}$$

The interface recombination velocities $v_{e/h}^{iface-SRH}$ are based on the material parameter and trap occupation is calculated using equation (4.77).

4.5.8 *Spontaneous Recombination*

Radiative recombination processes included spontaneous and stimulated recombination. With $Z(\omega)$ is the photon spectral density of states, the spontaneous recombination can be written as [85]

$$R^{spon,bound} = \int d\omega Z(\omega) u(\omega) \tag{4.79}$$

where u is the spontaneous emission spectrum. In QWs, it can be derived from the optical matrix element obtained from the bandstructure calculation. As in bulk regions and for continuum states, an approximate expression is used that is

$$R^{spon,bulk} = B\left(n_e n_h - n_i^2\right) \tag{4.80}$$

The Einstein coefficient B is based on material parameter.

4.5.9 *Stimulated Recombination*

Stimulated emission is the dominant radiative recombination above the laser threshold. The stimulated recombination is given by contributions due to photon emission into individual cavity modes (m, ω) [85]. The $g(\omega)$ is the gain spectrum.

$$R^{stim} = \sum_{m,\omega} S_{m,\omega} \left| E_m \right|^2 \frac{c}{n_{eff,m}} g(\omega) \tag{4.81}$$

4.5.10 *Carrier Current and Mobility*

The current densities $J_{e/h}$ in the carrier continuity equation below are calculated within the drift-diffusion theory where $D_{e/h}$ is the diffusivity, $\mu_{e/h}$ is the mobility and $P_{e/h}$ is the thermoelectric power of electrons and holes [85].

$$J_{e/h} = \pm qD_{e/h}\nabla n_{e/h} + q\mu_{e/h} n_{e/h} \nabla E_{C/V} \pm q\mu_{e/h} n_{e/h} P_{e/h} \nabla T \tag{4.82}$$

For Fermi statistics, the diffusivity is related to the carrier mobility through a generalized Einstein relation [85]

$$\frac{D_{e/h}}{\mu_{e/h}} = \frac{k_B T}{q} \frac{F_{1/2}\left(\frac{\pm F_{e/h} \mp E_{C/V}}{k_B T} \right)}{F_{-1/2}\left(\frac{\pm F_{e/h} \mp E_{C/V}}{k_B T} \right)} \tag{4.83}$$

The high-field mobility is written as a function of the low-field behavior and the electric field for electrons and holes [85]

$$\mu_{e/h} = \mu_{e/h}^{HF}\left(\vec{E}, \mu_{e/h}^{LF} \right) \tag{4.84}$$

4.5.11 *Temperature Dependent Mobility*

Temperature dependence is accounted using the expression below where the exponent $\delta_{0,e/h}$ and $\mu_{0,e/h}$ are based on material parameters for electrons and holes [85].

$$\mu_{e/h}^{LF} = \mu_{0,e/h}\left(\frac{T}{300K} \right)^{\delta_{0,e/h}} \tag{4.85}$$

The temperature dependence is induced by increased phonon scattering for increased temperature leading to exponents, and smaller than zero for most materials.

4.5.12 *Doping and Temperature Dependent Mobility Model*

This doping and temperature dependent mobility was originally modeled for Silicon devices and later developed to cover compound materials [88]. Due to impurity scattering, the carrier mobility generally exhibits a dependence on the doping concentration. The low-field mobility is given by [85]

$$\mu_{e/h}^{LF} = \mu_{dop,e/h}\left(\frac{T}{300K}\right)^{\delta_{dop,e/h}} + \frac{\mu_{0,e/h}\left(\frac{T}{300K}\right)^{\delta_{0,e/h}} - \mu_{dop,e/h}\left(\frac{T}{300K}\right)^{\delta_{dop,e/h}}}{1+\left(\frac{N_{dop}}{N_{ref,e/h}\left(\frac{T}{300K}\right)^{\delta_{ref,e/h}}}\right)^{\alpha_{e/h}\left(\frac{T}{300K}\right)^{\delta_{\alpha,e/h}}}} \tag{4.86}$$

where $N_{dop}=N_A+N_D$ is the total doping concentration. The maximum mobility $\mu_{0,e/h}$ and its exponent for the temperature dependence are described before. For increasing doping, the mobility approaches the minimum mobility $\mu_{dop,e/h}$. The temperature dependence of this minimum mobility is characterized by exponents $\delta_{dop,e/h}$. The reference doping density is $N_{ref,e/h}$ with its temperature dependence is described by the exponent $\delta_{ref,e/h}$.

4.5.13 *High Field Mobility*

The high-field mobility accounts for velocity saturation effects of the carriers. The model for the high-field behavior of the electron and hole mobility is given by [85]

$$\mu_{e/h}^{HF}\left(\vec{E},\mu_{e/h}^{LF}\right) = \frac{\mu_{e/h}^{LF}}{\sqrt[\beta_{e/h}]{1+\left(\frac{\mu_{e/h}^{LF}\left|\vec{E}\right|}{v_{sat,e/h}}\right)^{\beta_{e/h}}}} \tag{4.87}$$

The saturation velocity $v_{sat,e/h}$ for electron and hole are modeled using [85]

$$v_{sat,e/h}(T) = \frac{v_{sat,e/h}(300K)}{(1-a_{sat})+\frac{a_{sat}T}{300K}} \tag{4.88}$$

The temperature dependence coefficient a_{sat} and exponent $\beta_{e/h}$ are based on material parameter. In compound materials, electron mobility may exhibit a local maximum at high electric field modeled below with field strength $E_{HF,e/h}$ based on the material.

$$\mu_{e/h}^{HF}\left(\vec{E},\mu_{e/h}^{LF}\right)=\frac{\mu_{e/h}^{LF}+\frac{v_{sat,e/h}\left|\vec{E}\right|}{E_{HF,e/h}^{3}}}{1+\left(\frac{\left|\vec{E}\right|}{E_{HF,e/h}}\right)^{4}} \tag{4.89}$$

4.5.14 *Material Interfaces*

While the electric potential is continuous at material interfaces, different physical effects have to be considered for the carrier transport. Due to band discontinuities $\Delta E_{C/V}$ electrons and holes might encounter an energy barrier. Carriers with kinetic energy exceeding the barrier height are described by thermionic emission. The current is given below with A and B indicating wide and narrow gap materials [85].

$$J_{e/h,A\to B}=\frac{k_B^2 m_{e/h}^{*}}{2\pi^2\hbar^3}\left[\exp\left(\frac{F_{e/h,A}-E_{C/V,A}}{k_BT}\right)-\exp\left(\frac{F_{e/h,B}-E_{C/V,B}-\Delta E_{C/V}}{k_BT}\right)\right] \tag{4.90}$$

where $m_{e/h}^{*}$ is the carrier mass in the higher band edge material. As for carriers with insufficient energy to cross the interface, it generates quantum mechanical tunneling. A simple approach accounts for tunneling by reducing the barrier height as a function of the electric field to reflect increased tunneling probability for increasing electric field strength is given below with λ_{tunnel} is the effective tunneling length and $\vec{E}\vec{n}_{surf}$ is the projection of the electric field onto the surface normal at the interface.

$$\Delta E'_{C/V}=\Delta E_{C/V}-q\lambda_{tunnel}\max\left(0,\vec{E}\vec{n}_{surf}\right) \tag{4.91}$$

4.5.15 *Lattice Heat Flow Equation*

A fraction of electronic energy may be transferred to the crystal lattice due to carrier-phonon scattering, leading to lattice temperature increment. A lattice heat flow equation

can be solved to describe self-heating effects as below. The $C_L = c_L \rho$ is the lattice heat capacity, which is the product of specific heat and material density.

$$\left(C_L + \frac{3}{2} k_B \left(n_e + n_h\right)\right) \frac{\partial T}{\partial t} = \nabla\left(\kappa_L \nabla T - \vec{S}_e - \vec{S}_h\right) + H \tag{4.92}$$

4.5.16 *Thermal Conductivity*

The heat conductivity of the lattice have temperature dependence where the thermal conductivity at 300 K and the exponent δ_{κ_L} are based on the material as given by [85]

$$\kappa_L(T) = \kappa_L(300K)\left(\frac{T}{300K}\right)^{\delta_{\kappa_L}} \tag{4.93}$$

4.5.17 *Energy Flux*

The electron and hole energy fluxes are given by [85]

$$\vec{S}_{e/h} = \mp P_{e/h} T \vec{J}_{e/h} - \kappa_{e/h} \nabla T \tag{4.94}$$

The thermal conductivities of the electron and hole gas are determined by [85]

$$\kappa_{e/h} = n_{e/h} k_B T \mu_{e/h} P_{e/h} \tag{4.95}$$

4.5.18 *Heat Sources*

The sum of different heat source contributions, H in equation (4.92) is given as

$$H = H_{Joule} + H_{recombination} + H_{transient} \tag{4.96}$$

with the heat generation due to Joule heat H_{Joule}, recombination heat $H_{recombination}$ and an additional heat production rate originating from the transient modulation of the carrier concentration $H_{transient}$ expressed as [85]

$$H_{Joule} = -\frac{1}{q}\left(\vec{J}_e \nabla F_e + \vec{J}_h \nabla F_h\right) \tag{4.97}$$

$$H_{recombination} = \left(F_e - F_h\right) R^{dark} \tag{4.98}$$

$$H_{transient} = -T\left(\frac{\partial F_e}{\partial T}\frac{\partial n_e}{\partial t} + \frac{\partial F_h}{\partial T}\frac{\partial n_h}{\partial t}\right) \tag{4.99}$$

The sum of Peltier and Thomson heat as defined below is included in the convective part of the energy fluxes in equation (4.64) [85].

$$H_{P+T} = -\vec{J}_e T \nabla P_e - \vec{J}_h T \nabla P_h \tag{4.100}$$

4.5.19 *Thermal Boundary Conditions*

Two different boundary conditions can be associated with the heat flow equation at the electrodes contact. Firstly, it is treated as a reflective boundary and secondly, a Cauchy type boundary condition is imposed at the contact as defined by [85]

$$\kappa_L \vec{n} \nabla T = \frac{G_{thermal}}{A}\left(T - T_{contact}\right) \tag{4.101}$$

where $\vec{n}$ is the surface normal at the contact, A is the contact surface area, $G_{thermal}$ is the heat conductance associated with the electrode and $T_{contact}$ is the heat sink temperature.

4.6 Model for Spectral Broadening

Due to the intraband scattering, the electron and hole states during radiative transitions are not stationary and hence their energies are not certain. Finite coherence time of the states and uncertainty in the energy result in broadening of the spectral line. This spectral broadening is included by replacing the energy-delta function for transition probability from perturbation theory by following functions, which approaches a delta-function as the coherence time increases to infinity [82]

$$\delta\left(E_f - E_i - \hbar\omega\right) \rightarrow \delta_\Gamma\left(E_f - E_i - \hbar\omega\right) \tag{4.102}$$

Here, E_i and E_f are the energies of initial and final states, $\hbar\omega$ is the photon energy and Γ is the broadening parameter, related to the coherence time τ of a pair of the states involved in transition by $\Gamma = 2\pi\hbar/\tau$. In the limit of $\Gamma \rightarrow 0$, the broadened delta-function can be approximated by Lorentzian function at $\left|E_f - E_i - \hbar\omega\right| \ll \Gamma$. Instead of the energy delta-function, the Lorentzian broadened delta-function is used, that is [82]

$$\delta_{\Gamma}\left(E_f - E_i - \hbar\omega\right) = \frac{1}{\pi}\frac{\Gamma/2}{\left(E_f - E_i - \hbar\omega\right)^2 + \left(\Gamma/2\right)^2} \tag{4.103}$$

4.7 Model for Material Parameters

All of the material parameters employ in this modeling and simulation work are based on reliable experimental data and from literature sources [64, 89-100, 115]. The constants of the following materials GaAs, AlAs, AlGaAs, SiC, MgO, InGaAsP and InP are available in reference [86] and [115] respectively.